Optimal Control of Film Casting Processes

K. Selvanayagam* Thomas Götz†

Abstract

We present an optimal control approach for the isothermal film casting process with free surfaces described by averaged Navier–Stokes equations. We control the thickness of the film at the take–up point using the shape of the nozzle. The control goal consists in finding an even thickness profile. To achieve this goal, we minimize an appropriate cost functional. The resulting minimization problem is solved numerically by a steepest descent method. The gradient of the cost functional is approximated using the adjoint variables of the problem with fixed film width. Numerical simulations show the applicability of the proposed method.

1 Introduction

Polymer films for video and magnetic tapes are produced by film casting. The molten polymer emerging from a flat die is first stretched a short distance between the die and a temperature controlled roll. The film shows a lateral neck–in as well as an inhomogeneous decrease of the thickness. The formation of edge beads surrounding a central area of constant thickness is generally called the dog bone defect or edge bead defect. In this paper we develop an mathematical model to predict the shape of the die which minimizes the edge bead defect.

The paper is organized as follows: In Section 2 we expain the mathematical model describing the film casting process in an isothermal situation. In Section 3, the first order optimality system is introduced. Numerical methods and simulation results for both the state system and the optimization problem are presented in Section 4. We close with an outlook on open questions for future research.

2 Modelling film casting processes

In this paper we consider the stationary three–dimensional Newtonian, isothermal model for the film casting process, derived earlier by Demay and co–workers [1, 2, 4] or in [3]. The geometry of the film casting process is shown in Figure 1. During the film casting process, polymer is pressed through a nozzle or die (located in the yz–plane) with a velocity u_0 and wrapped up (velocity $u_L > u_0$) by a spindle at $x = L$. The nozzle has a width of W_0 in the y–direction and a thickness of e_0 in the z–direction. For typical film casting processes, the thickness of the film at the nozzle is small compared to both, the length and the width of the film, i.e. $e_0/W \ll 1$ and

*IIT Madras, Chennai 600036, India. email:kselva@iitm.ac.in
†Corresponding author, TU Kaiserslautern, Germany. email:goetz@mathematik.uni-kl.de

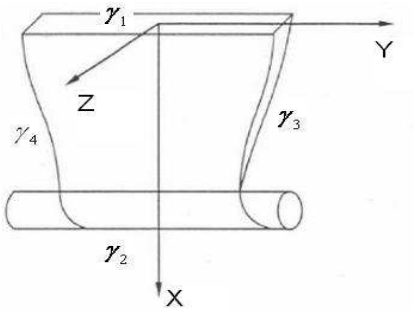

Figure 1: Sketch of the considered geometry for the film casting process.

$e_0/L \ll 1$. In this thin film limit, we average the mass and momentum equations describing the polymer flow over the z–direction. This leads to the following reduced equations, see [1, 2]

$$\nabla \cdot (eU) = 0 \tag{1a}$$

$$(U \cdot \nabla)U = \frac{1}{\mathrm{Re}} \left(\Delta U + 3\nabla \left(\nabla \cdot U\right)\right) \ . \tag{1b}$$

Here $U = (u, v)$ denotes the velocity field in the x– and y–directions and e denotes the thickness of the film in the z–direction. The Reynolds–number $\mathrm{Re} = \frac{Lu_L}{\nu}$ is based on the length of the film, the take–up velocity and the viscosity of the fluid. Using the notations of Figure 1, the system (1) has to be solved inside the two–dimensional film domain $\Omega = \{(x, y) : \ 0 < x < L \ , \ -W(x) < y < W(x)\}$. Note, that the width $W(x)$ of the film is a free boundary and not known a–priori. The boundary of the domain consists of the extrusion line $\gamma_1 = \{0\} \times (-W(0), W(0))$, the take–up line $\gamma_2 = \{L\} \times (-W(L), W(L))$ and the lateral boundaries $\gamma_3 = (0, L) \times \{-W(x)\}$ and $\gamma_4 = (0, L) \times \{W(x)\}$.

At the inflow boundary, we prescribe a fixed inflow velocity and the initial film thickness

$$(u, \, v, \, e) = (u_0, \, 0, \, e_0) \quad \text{at } \gamma_1 \ . \tag{2a}$$

And the spindle, we also prescribe the winding velocity

$$(u, \, v) = (u_L, \, 0) \quad \text{at } \gamma_2 \ . \tag{2b}$$

The ratio $D = u_L/u_0 > 1$ between the winding and the extrusion velocity is also known as the draw ratio. Due to the hyperbolic nature of Eqn. (1a), there is no boundary condition for the thickness on γ_2. The treatment of the lateral boundaries γ_3, γ_4 is more sophisticated, since they are free boundaries. Their location is not known in advance and evolves with the width $W = W(x)$ of the film. The dynamic and kinemetic conditions along the free boundary read as

$$\sigma \cdot n = 0 \quad \text{at } \gamma_3, \, \gamma_4 \ , \tag{2c}$$

$$u\partial_x W - v = 0 \quad \text{at } \gamma_3, \gamma_4 \ . \tag{2d}$$

Here n denotes the unit outer normal to γ_i, $i = 3, 4$ and

$$\sigma = (\nabla U) + (\nabla U)^T + 2\left(\mathrm{div}\, U\right) I = \begin{pmatrix} 4\partial_x u + 2\partial_y v & \partial_y u + \partial_x v \\ \partial_y u + \partial_x v & 2\partial_x u + 4\partial_y v \end{pmatrix}$$

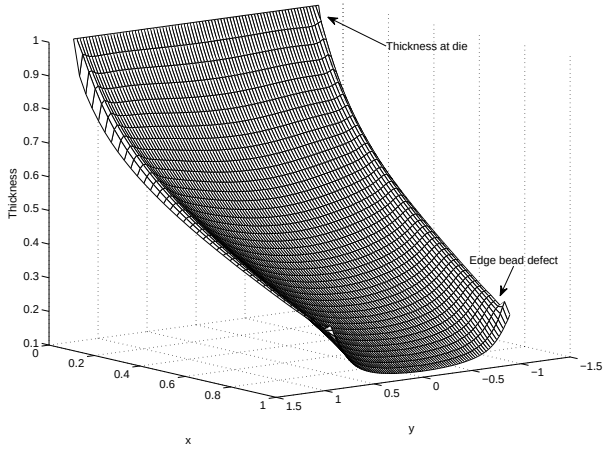

Figure 2: Thickness profile of the film casting process with edge bead defect.

is the stress–tensor and I is the 2×2 identity matrix.

To simplify notations, we call $z = (u, v, e)$ the state variables of the the problem.

Typical parameters used throughout the paper are given in the following table

stretching distance	$L = 0.4\,\mathrm{m}$
film width	$W = 1\,\mathrm{m}$
draw ratio	$D = 10$
Reynolds number	$Re = 3$

3 Optimal control

The model (1) is capable to predict the final thickness $e(L, y)$ of the film. This thickness profile depends on the geometry e_0 of the nozzle as well as the draw–ratio D. Using a rectangular nozzle, i.e. a uniform initial thickness e_0, one obtains the well–known effect of edge beads, see Figure 2. In this case the final film is thinner in the middle than at the lateral surfaces; an undesired result. In contrast to that, industrial applications aim to produce films with a uniform thickness profile at the take–up roll.

The parameters that can be modified are the initial thickness profile e_0 and the velocity at the die u_0 as well as the velocity of the take–up roll u_L. However, changing the constant velocity at the die or the take–up roll to a non–constant velocity profile is almost impossible under production conditions. Hence we focus on controlling the initial thickness $\varphi = e_0$ of the film.

To model the requirement of an even film thickness at the take–up roll, we consider the following tracking–type cost functional

$$J(z, \varphi) = \int_{-W(L)}^{W(L)} |e(L, y) - e_d|^2 \, dy \tag{3}$$

where e_d is the desired thickness.

The question of minimizing our cost functional $J(z, \varphi)$ belongs to the class of constrained optimization problem, where the cost functional (3) is minimized with respect to the constraint given by the state system (1),

$$\text{minimize } J(z, \varphi) \text{ with respect to } \varphi \text{ subject to (1).} \tag{4}$$

Optimization problems with differential equations constraints have gained a huge interest in the recent years, see [5, 6]. Optimal control problems for the Navier–Stokes equations, or models arising from them, have been investigated in [7, 8]. However, problems with free boundaries are yet a field of research and not much is known about general methods for this situation [9, 10].

In the sequel, we will formally introduce the Lagrangian for the problem (4). The first–order optimality system can be derived and leads to the problem of finding the adjoint operator for the state equations (1).

3.1 The first–order optimality system

Let Z denote the space of the state variables $z = (u, v, e)$ and C be the set of admissible controls, i.e. admissible nozzle shapes. To shorten the notation, we write the state system (1) together with its boundary conditions (2) shortly as $P(z, \varphi) = 0$, where $P : Z \times C \to W^*$ is called the state operator. Using a set $\xi = (\xi_u, \xi_v, \xi_e) \in W$ of Lagrangian multipliers, we introduce the Lagrangian $L : Z \times C \times W \to \mathbb{R}$ by

$$L(z, \varphi, \xi) = J(z, \varphi) + \langle P(z, \varphi), \xi \rangle_{W^*, W} \ . \tag{5}$$

Here $\langle p, \xi \rangle_{W^*, W} \in \mathbb{R}$ denotes the duality pairing between $p \in W^*$ and $\xi \in W$.

Now, as a standard result from nonlinear optimization, the Karush–Kuhn–Tucker (KKT) system is a necessary first–order optimality condition. Assuming enough regularity, the Lagragian is Fréchet–differentiable and the first–order optimality condition reads as

$$DL(z, \varphi, \xi) = 0 \ ,$$

or componentwise

$$P(z, \varphi) = 0 \quad \text{in } W^* \ , \tag{6a}$$

$$\partial_z P^*(\xi)[z, \varphi] + \partial_z J(z, \varphi) = 0 \quad \text{in } Z^* \ , \tag{6b}$$

$$\partial_\varphi P^*(\xi)[z, \varphi] + \partial_\varphi J(z, \varphi) = 0 \quad \text{in } C^* \ . \tag{6c}$$

In the system (6), we can easily identify the state (6a), adjoint (6b) and gradient equation (6c) in operator form.

Remark 3.1. To solve the KKT–system (6), we need to derive the adjoint equation (6b) in its strong or at least weak form. Here, the existence of the free boundaries γ_3, γ_4 poses a severe difficulty. Hence, we will derive in the sequel the adjoint equation for our model in the case of fixed boundaries.

This simplification is motivated by the observation, that the adjoint variables, as solution of the adjoint equation, are only needed to compute the direction of the gradient in (6c). When applying a numerical minimization algorithm to (4), we may also work with an inexact, only approximative gradient direction. Hence, we may replace the full adjoint problem, originating for the free boundaries, by a simpler, more tractable one with fixed boundaries. In Section 4, when we present

numerical results, we will a–posteriori justify this approch. We will see then, that our algorithm, based only on the inexact gradient information, sucessfully reduces the cost functional and terminates with a satisfactory solution for the minimization problem.

To derive the adjoint system and gradient equation, we rewrite the state problem (1) in weak form, multiply by the adjoint variables and integrate over the fixed domain $[0, L] \times [0, W]$. Then we apply the boundary conditions (2a), (2b) and (2c) which reads in the case of fixed boundaries γ_3 and γ_4 as

$$\partial_x u + 2\partial_y v = 0 \,, \qquad \partial_y u + \partial_x v = 0 \,. \tag{7}$$

Differentiation with respect to the state variables z yields the system of adjoint equations. Assuming enough regularity, we can identify the following strong form

$$u\partial_x \xi_e + v\partial_y \xi_e = 0 \tag{8a}$$

$$\frac{1}{Re}\left[4\partial_{xx}\xi_u + \partial_{yy}\xi_u + 3\partial_{xy}\xi_v\right] + u\partial_x\xi_u + \partial_y\left(v\xi_u\right) - \partial_x v\,\xi_v = e\partial_x\xi_e \tag{8b}$$

$$\frac{1}{Re}\left[\partial_{xx}\xi_v + 4\partial_{yy}\xi_v + 3\partial_{xy}\xi_u\right] + \partial_x\left(u\xi_v\right) + v\partial_y\xi_v - \partial_y u\,\xi_u = e\partial_y\xi_e \tag{8c}$$

together with the boundary conditions

$$\xi_e(L, y) = \frac{2\left(e(L, y) - e_d\right)}{u_L} \tag{8d}$$

$$\xi_u(0, y) = \xi_v(0, y) = 0 \qquad \xi_u(L, y) = \xi_v(L, y) = 0 \tag{8e}$$

$$\frac{1}{Re}\left[\partial_y\xi_u - \frac{7}{2}\partial_x\xi_v\right] + v\xi_u = 0 \quad \frac{4}{Re}\left[\partial_x\xi_u - \partial_y\xi_v\right] - v\xi_v = e\xi_e \quad \text{on } \gamma_3 \;\&\; \gamma_4 \tag{8f}$$

Taking the derivative of the Lagrangian L with respect to the control variable e_{in} yields the gradient equation

$$\int_0^W \xi_e(0, y)\, u_0\, e_{in}(y)\, dy = 0 \,. \tag{9}$$

4 Numerical Simulations

The KKT–system (6) corresponding to the first–order optimality conditions for the minimization problem (4) are a system of coupled, nonlinear PDEs. Hence, we will apply an iterative algorithm to solve them.

4.1 Solution algorithm

Starting from an initial guess for e_{in} we compute the state variables z from the nonlinear state equations. With this new state one can continue to solve the adjoint system for ξ. Using the state and adjoint variable we are able to update the control variable e_{in}. The detailed algorithm reads as

1. Given an initial control e_{in}^0. Set $k = 0$.
2. Solve the state equations (6a), i.e. (1) with the boundary conditions (2) as a free boundary value problem to obtain the new state variables z^{k+1}.

3. Given the state z^{k+1} corresponding to the control e_{in}^k, solve the adjoint problem (6b), i.e. (8) as a fixed boundary value problem to obtain ξ^{k+1}.

4. Given ξ^{k+1}, update the control by

$$e_{in}^{k+1}(y) = e_{in}^k(y) - \xi_e^{k+1}(0,y)\, u_0 \tag{10}$$

5. Calculate the cost functional $J^{k+1} = J(z^{k+1}, \varphi^{k+1})$

6. If $J^{k+1} < \epsilon$
then *Stop*
else set $k = k+1$ and go to step 2.

4.2 Solving the state equation

Since the boundaries γ_3 and γ_4 are free surfaces, it is difficult to implement the boundary condition $\sigma \cdot n = 0$. To overcome the free surface, we transform the domain into a square domain by mapping the coordinates (x, y) to $(x, \tilde{y})$ where $\tilde{y}(x) = \frac{y}{W(x)}$. Then, the new coordinates belong to a square domain $(x, \tilde{y}) \in [0, L] \times [-1, 1]$. Applying this coordinate transformation to the state system (1) yields

$$\partial_x(eu) - \tilde{y}\frac{W'}{W}\partial_y(eu) + \frac{1}{W}\partial_y(ev) = 0 \tag{11a}$$

$$\begin{aligned} u\partial_x u + \frac{v}{W}\partial_{\tilde{y}} u - u\tilde{y}\frac{W'}{W}\partial_{\tilde{y}} u = \frac{1}{\mathrm{Re}}\Bigg[& 4\partial_{xx}u + \frac{1}{W^2}\partial_{\tilde{y}\tilde{y}}u + \frac{3}{W}\partial_{x\tilde{y}}v - 8\tilde{y}\frac{W'}{W}\partial_{x\tilde{y}}u \\ & -4\tilde{y}\frac{W''}{W}\partial_{\tilde{y}}u + 4\tilde{y}\frac{(W')^2}{W^2}\partial_{\tilde{y}}u + 4\tilde{y}^2\frac{(W')^2}{W^2}\partial_{\tilde{y}\tilde{y}}u - 3\tilde{y}\frac{W'}{W^2}\partial_{\tilde{y}\tilde{y}}v - 3\frac{W'}{W^2}\partial_{\tilde{y}}v\Bigg] \end{aligned} \tag{11b}$$

$$\begin{aligned} u\partial_x v + \frac{v}{W}\partial_{\tilde{y}} v - u\tilde{y}\frac{W'}{W}\partial_{\tilde{y}} v = \frac{1}{\mathrm{Re}}\Bigg[& 4\partial_{xx}v + \frac{4}{W^2}\partial_{\tilde{y}\tilde{y}}v + \frac{3}{W}\partial_{x\tilde{y}}u - 2\tilde{y}\frac{W'}{W}\partial_{x\tilde{y}}v \\ & -\tilde{y}\frac{W''}{W}\partial_{\tilde{y}}v + \tilde{y}\frac{(W')^2}{W^2}\partial_{\tilde{y}}v + \tilde{y}^2\frac{(W')^2}{W^2}\partial_{\tilde{y}\tilde{y}}v - 3\tilde{y}\frac{W'}{W^2}\partial_{\tilde{y}\tilde{y}}u - 3\frac{W'}{W^2}\partial_{\tilde{y}}u\Bigg] \end{aligned} \tag{11c}$$

Since the flow is symmetric about the centerline $y = 0$, it is sufficient to solve the problem in the half domain $[0, L] \times [0, 1]$. The boundaries of the computational domain are the extrusion line $\gamma_1 = \{0\} \times [0, 1]$, the take–up line $\gamma_2 = \{L\} \times [0, 1]$ and the former free surface $\gamma_3 = [0, L] \times \{1\}$. The fourth boundary $\gamma_4 = [0, L] \times \{0\}$ is the symmetry line. The conditions at the boundaries read as

$$u = u_0\,, \qquad v = 0\,, \qquad e = e_0 \qquad \text{at } \gamma_1 \tag{12a}$$

$$u = u_L\,, \qquad v = 0\,, \qquad \text{at } \gamma_2 \tag{12b}$$

$$u(x,y) = u(x,-y)\,, \quad v(x,y) = -v(x,-y)\,, \quad e(x,y) = e(x,-y) \qquad \text{at } \gamma_4 \tag{12c}$$

$$\frac{1}{W}\partial_{\tilde{y}} u + \partial_x v - \tilde{y}\frac{W'}{W}\partial_{\tilde{y}} v = 0\,, \qquad \frac{2}{W}\partial_{\tilde{y}} v + \partial_x u - \tilde{y}\frac{W'}{W}\partial_{\tilde{y}} u = 0 \quad \text{at } \gamma_3 \tag{12d}$$

The film width $W(x)$ itself is computed using the kinematic condition (2d), i.e. $W' = v/u$ and $W(0) = W_0$.

In the numerical algorithm, we solve the system (11b) and (11c) for the velocities u and v. Afterwards, we update the film width W. These steps are iterated until convergence is reached. Then, we compute the film thickness using (11a).

Remark 4.1. If we use the system (11) and (12) to derive the adjoint and gradient equation, we get the exact adjoint gradient equation. However, the adjoint system will have a rather complicated structure and hence it will be difficult and expensive to solve. Therefore, we prefer to work with the inexact adjoint system (8) which is cheaper to solve. The price for the reduced complexity of the adjoint system is an increase of the number of iterations needed to solve the full KKT–system (6).

4.3 Discretization

For the numerical simulations we use standard finite differences on a uniform grid with mesh widths h, $k > 0$ in the x– and $\tilde{y}$–direction resp. The same grid is used for the state as well as for the adjoint equation. We use the standard notation u_{ij} to denote the value of the function u at the grid point $(x_i, \tilde{y}_j) = (ih, jk)$. For the hyperbolic equations (11a) and (8a) we apply upwind methods. In equation (11a) governing the film thickness, the flow is oriented in the positive x–direction; hence the upwind scheme reads as

$$\frac{(eu)_{ij} - (eu)_{i-1j}}{h} - y\frac{W'}{W}\frac{(eu)_{ij+1} - (eu)_{ij-1}}{2k} + \frac{1}{W}\frac{(ev)_{ij+1} - (ev)_{ij}}{k} = 0\,.$$

In case of the adjoint thickness equation (8a) the information is travelling in the reverse direction and hence the upwind discretization reads as

$$u_{ij}\frac{(\xi_e)_{i+1j} - (\xi_e)_{ij}}{h} + v_{ij}\frac{(\xi_e)_{ij} - (\xi_e)_{ij-1}}{k} = 0\,.$$

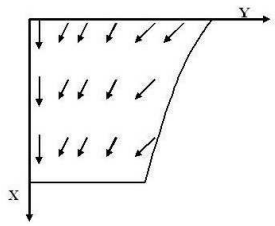

Figure 3: Flow direction in the state system.

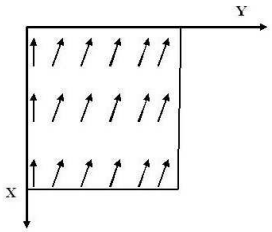

Figure 4: Flow direction in the adjoint system.

In the velocity equations (11b) and (11c) the nonlinear terms are handled by iteration. Central differences are used to discretize the derivatives. The adjoint equations (8b) and (8c) are discretized analogously.

4.4 Simulation Results

In a first step, we solved the state system (1) or resp. (11) for a given, constant initial thickness e_0. Figure 2 on page 3 shows the thickness of the film. The transversal velocity component v is shown in Figures 5 and 6. Figure 5 plots the transversal velocity $v(\cdot, y)$ at different lateral cuts $x = x_i$. Figure 6 contains the same velocity component, but at longitudinal cuts $y = y_j$.

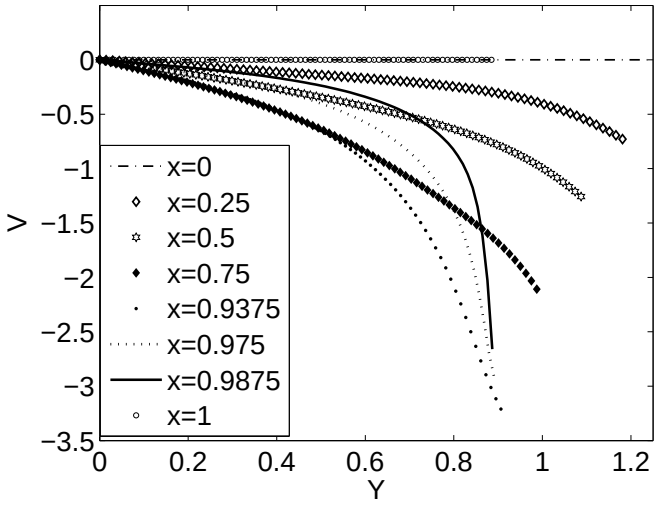

Figure 5: Transversal velocity v.

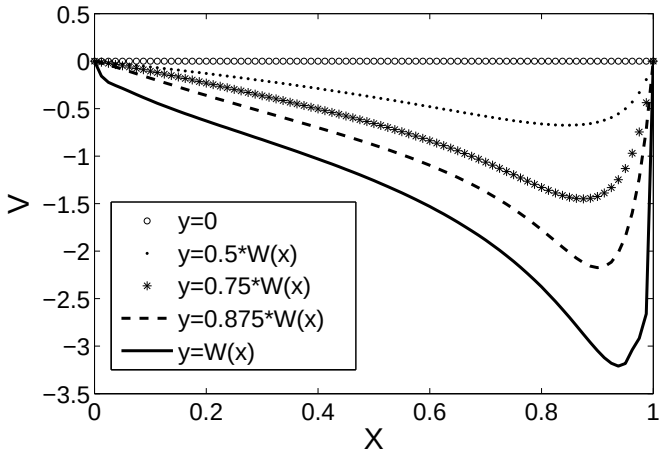

Figure 6: Transversal velocity v.

In Figure 5 the velocities are is negative, implying that the fluid moves towards the centerline $y = 0$; this yields the neck–in of the film. This neck–in is also clearly visible in Fig. 8 showing the evolution of the width of the film.

In Figure 6, the centerline of the film, i.e. $y = 0$, corresponds to the velocity $v = 0$ and the edge or boundary of the film corresponds to the curve with maximum velocity. Along the central part of the film, i.e. close to the centerline, the transversal velocity component v is rather small. Hence we may conclude, that in the central part of the film mainly uniaxial extension occurs, i.e. just a stretching in the longitudinal direction. Along the edges of the film, biaxial extension is predominant leading to a stretching and necking–in of the film.

Figure 7 shows the longitudinal velocity component $u(\cdot, y)$ at different lateral cuts, analogous to Fig. 5. The increase of the longitudinal velocity due to the draw ratio $D > 1$ is clearly visible.

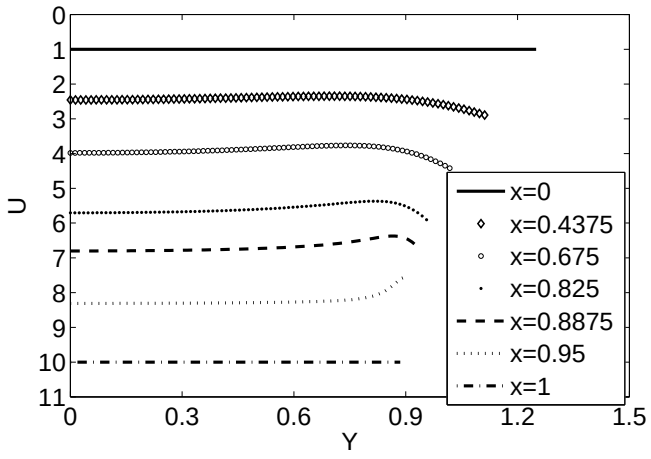

Figure 7: Longitudinal velocity u.

Finally, we investigated the result of the optimization problem (4). The aim was to find a shape of the nozzle, i.e. an initial thickness e_0 of the film, such that we obtain a uniform thickness e_d at the position of the spindel. Figure 9(A) shows the un–optimized situation. Lateral cuts of the film thickness $e(\cdot, y)$ are plotted for different x–coordinates along the film. Two effects are clearly visible from this figure: on the one hand the decrease of the film thickness along the centerline $y = 0$. And on the other hand the development of the edge–bead effect as the longitudinal coordinate x grows. In contrast to that, Fig. 9(B) shows the situation with the optimized initial thickness e_0. The uppermost line corresponds to the initial thickness e_0 and the graph at the bottom shows the film thickness at the take-up point $x = L$. At the take-up point we obtain a constant film thickness of $e_d = 0.1$ corresponding to the draw ratio $D = 10$. Figures 10 and 11 show a comparison of the un–optimized (left) and optimized situation (right). The initial thickness corresponding to the shape of the nozzle is shown in the upper part and the final film thickness is given below. In the optimized situation the close–to ellipsoidal shape of the nozzle counterbalances the edge–bead effect resulting in a uniform film thickness.

Remark 4.2. The results shown in Figs. 10 and 11 may serve as a a–posteriori justification of our inexact adjoint system (8). Recall, that we solve the state equation (1) as a free–boundary value problem, but the adjoint system on a fixed domain

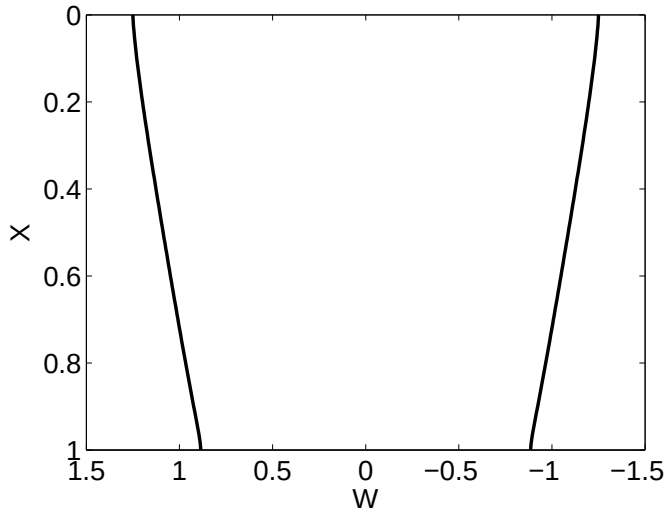

Figure 8: Film width w.

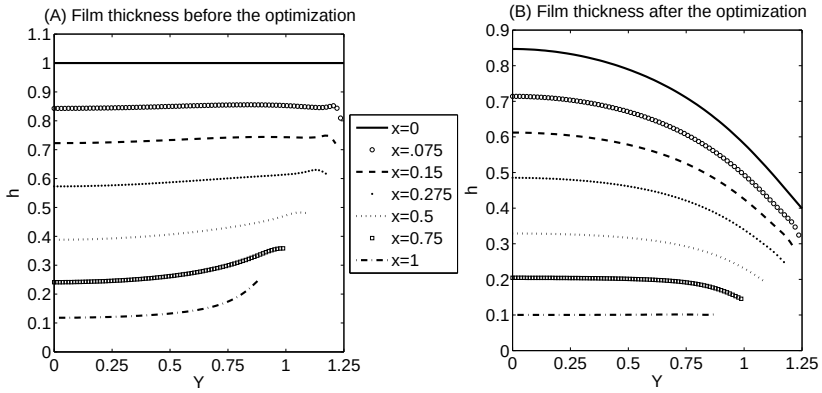

Figure 9: Film thickness e before the optimization (A) and after the optimization (B).

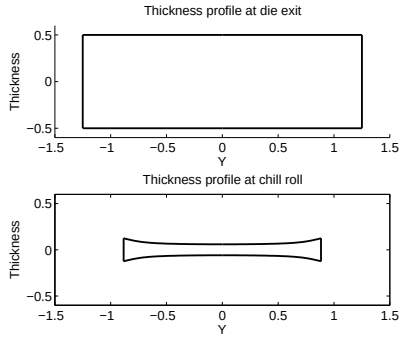

Figure 10: Nozzle shape (top) and film thickness at take–up (bottom) before the optimization.

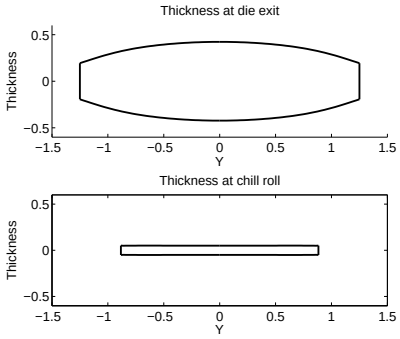

Figure 11: Nozzle shape (top) and film thickness at take–up (bottom) after the optimization.

with a uniform film width. This leads to an inexact computation of the gradient and hence an inexact update of the control variable in Eqn. (10). However, this inexact update still leads to a decrease in the cost functional and our optimization algorithm terminates with an acceptable solution, solving the problem (4). A rigorous justification of this observation based on space–mapping techniques is left open for future research.

To end our investigations of the optimization problem, the following table shows the computationl time and the number of iterations required for different tolerence levels ϵ.

ϵ	Number of Iterations	Time
.05	9	62.0 sec
.01	97	71.9 sec
.005	135	76.1 sec
.001	212	84.6 sec

5 Conclusion

We studied the isothermal film casting process. Based on the averaged Navier–Stokes equations, the evolution of the film thickness and width is governed by a free boundary value problem. In an industrial application of the film casting process, one is typically interested in obtaining an even thickness distribution at the take–up point of the film. However, a uniform thickness profile at the nozzle always leads to the so–called edge–bead effect; the final film gets thinner in the middle than at the edges. Hence we formulated an optimization problem to determine the optimal shape of the nozzle, that will lead to an even thickness distribution at the take–up point. Applying the Lagrangian formalism to a modified problem with fixed film width, we were able to derive an approximate adjoint equation. This approximate adjoint was used to set-up an minimization algorithm for our problem. Numerical simulations show, that even with this approximate version of the adjoint equations, the minimization algorithm converges. Therefore we were able to compute the optimal shape of the nozzle, that produces a uniform film thickness.

A mathematical analysis of the proposed approximative adjoint equations and their relation to the full adjoint equations for the free boundary value problem is left as an open question subject to future research.

References

[1] S. d'Halewyu, J. F. Agassant and Y. Demay, 'Numerical Simulation of the Cast Film Process', Polymer engineering and science, 30, 335–340 (1990).

[2] D. Silagy, Y. Demay and J. F. Agassant, 'Numerical simulation of the film casting process', Int. J. Numer. Meth. Fluids, 30, 1–18 (1999).

[3] P. Barq, J. M. Haudin and J. F. Agassant, 'Isothermal and Anisothermal Models for Cast Film Extrusion', Intern. Polymer Processing, VII(4), 334–349 (1992).

[4] A. Fortin, P. Carrier and Y. Demay, 'Numerical Simulation of Coextrusion and Film Casting', Int. J. Numer. Meth. Fluids, 20, 31–57 (1995).

[5] M. Hinze and S. Volkwein, 'Instantaneous Control for the Instationary Burgers Equation - Convergence Analysis & Numerical Implementation', Nonlinear Analysis T.M.A, 50, 1–26 (2002).

[6] H. Goldberg and F. Troeltzsch, 'On a Lagrange-Newton method for a nonlinear parablic boundary control problem', Optimization Methods and Software, 8, 225–247 (1998).

[7] F. Abergel and R. Temam, 'On Some Control Problems in Fluid Mechanics', Theoretical and Computational Fluid Dynamics, 1, 303–325 (1990).

[8] M. D. Gunzburger, L. S. Hou, S. Manservisi, Y. Yan, 'Computations of Optimal Controls for Incompressible Flows', International Journal of Computational Fluid Dynamics, 11, 181–191 (1998).

[9] M. Hinze and S. Ziegenbalg, 'Optimal control of the free boundary in a two–phase Stefan problem with flow driven by convection', ZAMM, 87 No. 6, 430–448 (2007).

[10] M. Hinze and S. Ziegenbalg, 'Optimal control of the free boundary in a two–phase Stefan problem', J. Comput. Phys., 223 No. 2, 657–684 (2007).